Melanoma Detection By AFM Indentation of Histological Specimens

ByoungJun Jeon
Seoul National University
Hyo Gi Jung
Korea University
Sang Won Lee
Korea University
Gyudo Lee
Korea University, Sejong
Jung Hee Shim
Seoul National University Bundang Hospital
Mi Ok Kim
Seoul National University College of Medicine
Byung Jun Kim
Seoul National University College of Medicine
Sang-Hyon Kim
Keimyung University Dongsan Medical Center
Hyungbeen Lee
Yonsei University
Dae Sung Yoon
Korea University
Seong Jin Jo
Seoul National University College of Medicine
Tae Hyun Choi
Seoul National University College of Medicine
Wonseok Lee (wslee@ut.ac.kr)
Korea National University of Transportation

Research Article

Keywords: atomic force microscopy (AFM), Gaussian distributions, heterogeneous, histopathological analysis, precise melanoma detection

DOI: https://doi.org/10.21203/rs.3.rs-917257/v1

Abstract

Melanoma is visible unlike other types of cancer, but it is still challenging to diagnose correctly because of the difficulty in distinguishing between benign nevus and melanoma. We conducted a robust investigation of melanoma, identifying considerable differences in local elastic properties between nevus and melanoma tissues by using atomic force microscopy (AFM) indentation of histological specimens. Specifically, the histograms of the elasticity of melanoma displayed multimodal Gaussian distributions, exhibiting the heterogeneous mechanical properties, in contrast with the unimodal distributions of elasticity in the benign nevus. We identified this notable signature was consistent regardless of blotch incidence by sex, age, anatomical site (e.g., thigh, calf, arm, eyelid, and cheek), or cancer stage (I, IV, and V). In addition, we found that the non-linearity of the force-distance curves for melanoma is increased compared to benign nevus. We believe that AFM indentation of histological specimens may technically complement conventional histopathological analysis for earlier and more precise melanoma detection.

Introduction

Melanoma is originated from aberrant melanin-pigmented cells and is responsible for approximately 80% of patient deaths from skin cancer [1,2]. Because the survival of melanoma depends strongly on whether cancer invades from the epidermis to the dermis, it is important to identify early-stage melanoma before the invasion. Commonly, the pathologic examination has been performed on histological specimens to determine whether they are benign or malignant, but this method often results in both false positives and false negatives [3,4]. Accordingly, other diagnostic techniques such as optical examination [5-7] and ultrasound [8,9] have been developed, but these are still inaccurate as well; in particular, they suffer from low sensitivity owing to either epidermal structures such as hair or scars or motion artifacts during measurement [10].

To overcome these limitations, researchers have developed complementary methods such as image processing and impedance measurement [8,11-15], but demarcating a boundary between a benign nevus and melanoma is still uncertain [16]. This uncertainty is thought to derive from the anatomical structure of the epidermis, where there is no extracellular matrix (ECM), so that melanoma tumorigenesis differs from that of other cancers [17,18]. Many cancers undergo ECM remodeling on progression (e.g., in stiffness and configuration) [19-22], but melanoma does not undergo this process due to the absence of the ECM. It indicates that melanoma tissue exhibits little discernable changes in morphological or physical properties compared to other cancers [23,24].

Given this consideration, we need to pay attention to the tumorigenesis that is specific to melanoma rather than other cancers, including the minute changes in the molecular interactions (e.g., melanin transfer and pigmentation). We believed that the tumorigenesis would modulate the mechanical properties of melanoma tissues in the interface between the epidermis and the dermis (i.e., nearby basal layers) [1,25,26]. The changes in the mechanical properties of melanoma tissues would then derive from the

cellular configuration changes within melanoma tissues in comparison with both nevus and normal tissues. However, with conventional methods, a sharp distinction between a benign nevus and malignant melanoma is still challenging [27,28].

Meanwhile, we noted the typical symptoms of melanoma blotches — irregular color, shape, or both — in the outermost layer of skin, whereas benign nevus revealed regular round shapes and uniform color (Fig. 1a), and this trend was consistent with a previous report that studied visual inspection [29]. Based on our visual inspection knowledge, our detailed rationale for the development of malignant melanoma with melanin transfer and pigmentation processes in the vicinity of a basal layer is as follows: i) in the epidermis, melanoma neoplasm develops from abnormal melanin transfer and pigmentation from the surrounding keratinocytes and melanocytes [30,31]; ii) in this process, the cell-cell junctions of keratinocytes acting as homogeneous melanin transfer pathways could be confined and thus drive the development of a benign pigmented area (i.e., a nevus) [1]; iii) in contrast, in melanoma development, melanin transfer and pigmentation become irregular by the invasion of melanoma cells, and the cell-cell junctions between cancer and normal cells act as heterogeneous melanin transfer pathways (Fig. 1b) [17,27]. Accordingly, subtle differences in neoplasm formation may lead not only to the different visual signatures of the skin blotches but also to the obvious contrast in the mechanical properties between nevus and melanoma tissues. Therefore, we hypothesized that distinct local elastic properties of both lesion tissues (benign nevus and malignant melanoma) are implicit in the biopsied specimens and can be measured (Fig. 1c). Recently, He *et al.* found a trend that melanoma tissue has higher density and more heterogeneous distribution patterns of melanin than benign tissue using the three-dimensional imaging of the tissue with confocal photothermal microscopy [32], which may support our hypothesis.

Up to date, biopsied cancer tissues have been employed for mechanical characterization. However, it has a limitation that the mechanical properties of tissues can change over time after biopsy [33-35]. The histological specimens, commonly used for diagnosis in hospitals, can overcome this difficulty in handling and the storing biopsied samples to study their mechanical properties [33]. These specimens can be easily handled and can be reused because they can withstand long-term storage due to fixed and mummified tissue. As such, our goals were to verify i) whether the mechanical characterization of histological specimen would be consistent with the results from conventional histopathological analysis and ii) whether it could provide abundant information about benign versus malignant epidermal tissues, complementing the traditional histopathological examinations.

Atomic force microscopy (AFM) is a multi-functional device that can analyze a sample's morphology, mechanical strength, and surface charge by its nano-scale cantilever [36-39]. In this report, we demonstrate a robust mechanical characterization of histological specimens using atomic force microscopy (AFM) indentation for discrimination among normal, benign nevus, and melanoma. Specifically, the histograms of the elasticity of melanoma displayed multimodal Gaussian distributions, exhibiting heterogeneous mechanical properties, in contrast with the normal and benign nevus. We also identified the mechanical characteristics of each histological specimen regardless of blotch incidence by sex, age, anatomical site

(e.g., thigh, calf, arm, eyelid, and cheek), or cancer stage (I, IV, and V). Moreover, we found that the non-linearity of the measured force-distance (FD) curves for melanoma specimens tends to be increased compared to normal and benign nevus. This implies that the non-linearity of FD curves will be another significant metrics for melanoma detection in cooperation with the elasticity mapping. We believe that the AFM indentation of the histological specimen can be considered a useful and complementary technique not only for providing an excellent complement to histopathological examination for precise diagnosis but also for predicting the invasiveness and ablation margin during oncological surgery.

Methods

Biopsy from Patients

All samples were collected from patients who need pathological evaluation at the Seoul National University Hospital. A total of 32 human biopsies of tissue samples were obtained from both males and females aged 1 to 81: 7 normal skin samples, 13 benign nevus samples, and 13 melanoma samples. The biopsies of each patient were evaluated by standard pathological procedures before conducting the AFM analysis, and the pathologists determined that among the 13 melanoma tissue samples, three were Clark level I, five were level IV, and the remainder were level V. Remaining sample blocks were then prepared for AFM analysis. Ethical approval was obtained from the Institutional Review Board of Seoul National University Hospital (IRB Approval Number: 1505-092-673). All experiments dealing with human or human products were conducted with informed consent and carried out in accordance with the relevant guidelines and regulations. The biopsies of each patient were evaluated by standard pathological procedures before we conducted the AFM analysis, and the pathologists determined that among the 13 melanoma tissue samples, three were Clark level I, five were level IV, and the remainder were level V. All experiments were performed by relevant guidelines and regulations.

Preparation of Histological Specimens

The acquired tissue samples were formalin-fixed and paraffin-embedded according to standard histological procedures. The prepared paraffin-embedded blocks were sectioned at roughly 4 μm thickness on a microtome and transferred onto glass slides suitable for immunohistochemistry. The first sections were stained with hematoxylin and eosin (H&E) and used for traditional histopathological examination using an upright light microscope (Leica Microsystems GmbH, Wetzlar, Germany) to determine the lesion. The second sections were also stained with H&E, but they were not mounted with a cover glass; the uncovered samples were used for AFM indentation after drying.

Histological Analysis

We determined the histologic lesions of benign nevus and melanomas where AFM topography was obtained, and AFM indentation was measured. Specifically, we determined that the benign nevus lesions were nests of melanocytes in the lower aspect of the epidermis in the H&E sections; the melanocytes were

ll nucleoli and clear to pale staining cytoplasm

containing evenly distributed melanin granules. In contrast, we determined the melanoma lesions to be areas where atypical melanocytes were scattered or formed clusters. These atypical melanocytes contained pleomorphic, angular, and hyperchromatic nuclei and showed conspicuous cytoplasmic fixation retraction artefacts. Pigmentation was often abundant, and multinucleate tumor cells were commonly seen.

AFM Topography of Histological Specimens

All histological specimens which were mummified samples after fixation of tissue were stored in a desiccator. The humidity (47%) of the laboratory was constantly maintained during all AFM indentation experiments. We acquired the AFM images for topological analysis of the histological specimens using commercial AFM (XE-Bio, Park Systems, Korea) operated in an air-conditioned environment; the image sizes were 60 × 60, 70 × 70, and 90 × 90 μm^2, and the scan rate was 0.5 Hz. Before the AFM imaging, we moved the cantilever above the tissue lesion using an optical microscope. We obtained and analyzed all AFM images and surface roughness data using the commercial Park Systems software, XEI version 4.3.0.

AFM Indentation of Histological Specimens

To investigate the mechanical properties of the histological specimens, we conducted the AFM indentation in air conditioning. For all of the indentation experiments, we used aluminum-coated cantilevers (PPP-NCHR, tip radius of curvature <10 nm, resonant frequency in air: 330 kHz) with spring constants of 38.70 ± 1.13 N/m and force sensitivity of 73.02 ± 0.83 V/μm. In all the indentation experiments, the cantilevers with the spring constant and force sensitivity were carefully chosen and used for measurement. For the tissue specimens, we conducted the AFM indentations in force-volume mode, wherein we collected an array (10 × 10 points) of FD curves over the entire scan area (30 × 30 and 45 × 45 μm^2, half of the full AFM image size). We acquired force–volume maps spaced 3 and 4.5 μm apart in a systematic manner across the entire mapping surface (Fig. 3g-i). In our experiment, each FD curve consisted of 512 data points. The cantilever was brought to the specimens with the constant speed of 1 μm/sec for the tissue specimens and 0.3 μm/sec for the cells, and it was held on the tissue surface at a constant force of 2 – 3.8 μN depending on the mechanical differences within the histological specimens. Note that the histological specimen could withstand the micro-newton force because it was a fixed tissue with chemical reagent rather than raw biological tissue. After the indentation experiment, we confirmed that no dramatic damage to the histological sample was observed using the charge-coupled device. We calculated the elasticity of each specimen through the measured FD curves, which we derived from the Hertz model provided in XEI.

Statistics

To investigate the statistical differences of our data, peaks of histograms were analyzed by the peak analyzer application of OriginPro 2016. The statistical significance of differences between peak values in histogram was assessed with the ANOVA in OriginPro, where significance was taken as $p < 0.05$.

Results

Surface Profiling of Histological Specimens by using AFM

Prior to our AFM indentation experiments, we performed AFM imaging for morphological analysis of histological specimens (Fig. 2a-c and Supplementary Fig. S1). The AFM micrographs showed circular or elliptical craters (approximately 10 μm), which are presumed to be cell markers (Fig. 2d-f). We found that the AFM topographies notably differed among normal, benign nevus, and melanoma. We believed that the higher density and correspondingly smaller sizes of the craters had evolved during nevus development, but there were still some aligned crater structures in the nevus specimens. In contrast, the melanoma showed irregular crater shapes, sizes, densities, and even alignments. These structural irregularities could have been formed during the transformation to malignancy [27,28], and it can affect the changes in the physical properties of the samples.

For the quantitative analysis beyond that of appearance, we compared the histograms of height distribution from each AFM micrograph in Fig. 2g-i. The standard deviations (σ) of the histograms, fitted to Gaussian distributions, are shown in Fig. 2j. In addition, we attempted to calculate the surface roughness (S_q) from the AFM micrographs, but we found that both metrics (i.e., σ and S_q) were ineffective at discriminating among normal, benign nevus, and melanoma (Fig. 2k and Supplementary Fig. S2). The results of morphological analysis were similar because the histological specimens were finely sectioned at the same thickness (4 μm). Although the microscopic analysis (i.e., AFM imaging) showed higher-resolution images compared with macroscopic inspection (e.g., simple visual inspection using ABCDE criteria), we comprehensively demonstrated the vulnerability of AFM image analysis for melanoma detection using histological specimens.

Mechanical Properties of Histological Specimens that can Discriminate Between Benign Nevus and Melanoma

To overcome the vulnerability of AFM image analysis, we performed AFM indentation of the histological specimens in the vicinity of the epidermis (Fig. 3a-c). The mechanical properties of specimens can be quantified by using FD curve measurements, which we acquired from 100 independent locations throughout the entire lesion. To confirm whether the histological specimen is softer than the substrate (i.e., glass) or not, we evaluated the mechanical properties of the glass substrate. We observed that the elasticity of the substrate that supported the histological specimens was exceeded the usual range of the mechanical properties of histological specimens, indicating that the heterogeneous properties of the histological specimens are not influenced by the substrate (Supplementary Fig. S3). Therefore, we were convinced that our experimental setup and the following results are reasonable.

All the FD curves are presented from the contact point to the maximum indentation depth in the form of approach curves after the contact point. The displayed FD curves (Fig. 3d-f) is a set of the approach curves where the contact points of the FD curves fit in the origin (d = 0 μm, F(d) = 0 μN). The majority of

FD curves from normal sample exhibited linear behavior during the indentation (Fig. 3d). The majority of FD curves from the benign sample showed relatively steeper slopes in the linear region than did the normal sample, implying that benign sample retains higher resistance to elastic deformation. It is noteworthy that a few of the FD curves in the benign sample revealed non-linear characteristics (Fig. 3e). In contrast, the FD curves for the melanoma specimen exhibited non-linear characteristics (Fig. 3f), suggesting that benign nevus is relatively harder than normal sample, whereas melanoma appears to combine softness and hardness. We will discuss the non-linear characteristics of FD curves in detail later in this article.

We conducted the stiffness mapping of the specimens; stiffness maps are derived from FD curves, and they show the deformation of samples. In our study, a representative stiffness map of a benign nevus revealed that overall stiffness was higher than that in the normal sample (Fig. 3g and h). In contrast, the stiffness map of the melanoma displayed randomly blended colors, indicating a mixture of soft and hard materials, unlike with normal or nevus sample (Fig. 3i). This suggests that the local elastic properties of melanoma are heterogeneous.

To quantify the extent of any heterogeneity, we calculated the elastic modulus (E_a) using the FD curve data. The average E_a in the normal sample was 401 ± 148 MPa, and that of the benign nevus was 575 ± 107 MPa. Here, we found two things: The elasticities of the benign nevus were generally 100 MPa higher than those of the normal sample, and the histograms of the elasticity distributions of the normal and benign samples followed Gaussian distributions with single peaks (Fig. 3j and 3k). In contrast, the elasticities of the melanoma were described by multiple Gaussian distributions (188 ± 78, 497 ± 110, and 787 ± 56 MPa; Fig. 3l). This result implies that the epidermis of melanoma consists of heterogeneous materials including soft matter. It is surprising because such mechanical characteristics are of tumor tissue with ECM [27,28,40]. Perhaps, the role of ECM in the tumorigenic process is seemed to replace with some factors (e.g., melanin transfer and pigmentation) in melanoma development. Meanwhile, we checked whether the samples would retain similar trends in elastic properties even after long periods of time, and this is of practical clinical importance as well; our AFM indentation testing verified that the characteristics of the melanoma such as the multimodal Gaussian distribution survived for more than three months (Supplementary Fig. S4). Previous studies have found that using histological specimens has a strong advantage in overcoming the weakness of the time-dependent biodegradation of biopsied tissues [35,41].

The results for the mechanical properties of all specimens are summarized in Table 1 and shown in Supplementary Fig. S6, S7, and S8. We found that the elasticities of all histological specimens could be separated into three segmented regions across the full range: the ranges were region I (0–300 MPa), region II (300–600 MPa), and region III (600–900 MPa). The different specimens' E_a value ranges depended on the specimens' origins; for instance, the E_as for all normal samples were in region II (300–600 MPa), exhibiting a single-mode Gaussian distribution, and the E_as for the benign nevus spread across regions II and III and displayed single-mode Gaussian distributions. However, the elasticities of the

melanoma exhibited multimodal Gaussian distributions that ranged from regions I to III and mainly consisted of three peaks (occasionally there were two peaks). It should be noted that this classification is highly useful in testing the versatility of our approach with all epidermal lesions regardless of sample type.

Table 1
Summary of mechanical analysis and histological examination of biopsied samples with patient information. The corresponding elasticity distributions are shown in Figure S6, S7, and S8).

Versatility of the Mechanical Specimen Signatures Regardless of Age, Sex, or Site

The epidermis is the outermost layer of the skin, which suggests that it can be easily deformed and that it has different mechanical properties depending on age, sex, and site [42,43]. To clinically apply our methodology, it was essential to verify whether the mechanical signatures for discrimination would hold constant irrespective of skin tissue type. Thus, we classified the mechanical properties of the specimens according to age (1–81 years), sex (male or female), and site (thigh, inguinal, cheek, leg, arm, back, flank, abdomen, and elbow). Surprisingly, the specimen signatures varied based on normal, benign nevus, or melanoma samples regardless of age, sex, or site (Fig. 4a-i). The average E_as for the normal and benign nevus samples fell in region II or regions II and III — showing single-mode Gaussian distributions — whereas those of the melanoma mostly had multiple peaks and were distributed throughout all the elastic regions (I, II, and III). In detail, the E_as for the normal samples ranged from 370 to 521 MPa, all within region II. The benign nevus had higher E_as, ranging from 441 to 848 MPa, in regions II and III. In contrast, the melanoma displayed three peak Gaussian distributions, and each peak had a different average: E_{1a} = 158–274 MPa (region I), E_{2a} = 363–542 MPa (region II), and E_{3a} = 606–893 MPa (region III).

Whether the melanoma cancer stage can distort the mechanical signatures is another important factor for determining the clinical applicability of our method. It is well-known that melanomas become darker, more distorted, and physically harder as the stage increases (Fig. 4j). Accordingly, we determined the cancer stage of each melanoma based on Clark level (see Methods) and then inspected all the melanoma by AFM indentation. Notably, all samples exhibited multiple Gaussian peaks; each E_a occupied its own elastic region (Fig. 4k). From our results, it is plausible that the mechanical signature of the multiple

peaks survives in melanoma irrespective of the cancer stage, even in stage I, and the existence of these multiple peaks in stage I melanoma provides us with a strong advantage in early detection.

At this stage, we needed to scrutinize in detail how the melanoma cancer stage affected its mechanical characteristics. One particular point is that unlike with other cancers, melanoma's mechanical properties appeared to vary significantly depending on the stage. Specifically, each of our melanoma samples showed a most prevalent peak (P_m) — one with the highest population — among its multiple peaks (Supplementary Fig. S9). We considered the P_m and its corresponding elastic region, I, II, or III, as important parameters. We conducted our statistical analyses of each category based on the two parameters above, and we present the results in Fig. 4l and Supplementary Fig. S9. We found no significant differences in the mechanical properties of melanoma by sex, age, or site. However, we found that the melanoma specimens tended to become harder as the cancer stage advanced. In particular, all early-stage (stage I) melanoma samples had their own P_m values, which were all in the region I, which implied that the specimens contained large amounts of soft material. However, in the late melanoma stages (IV and V), the P_m values ranged across all three elastic regions, I, II, and III. This finding indicates that at the late stage, hard material fills the samples in larger amounts than in the early stage. This phenomenon is consistent with the fact that melanin accumulates as the cancer stage advances [44]. Taking these findings together, although there were subtle differences by category and cancer stage, we found it surprising that all the melanoma samples still retained their mechanical signature of multiple Gaussian peaks.

Non-linearity of FD Curves for Normal, Benign Nevus, and Melanoma

Meanwhile, we paid attention that the FD curves for normal and benign nevus samples exhibited linear behavior whereas the FD curves of melanoma showed non-linear characteristics (Fig. 3). To quantitatively compare the non-linear characteristics of each sample, we calculated the non-linearity from FD curves as follows. As shown in Fig. 5a, we draw a straight line (red-dashed) between the contact-point (X_{min}, Y_{min}) and end-point (X_{max}, Y_{max}) in the FD curve. We define this straight line as the ideal curve (i.e., perfectly linear line):

$$\mathrm{Idealcurve}: \mathrm{y}_{\mathrm{linear}} = \frac{\mathrm{Y}_{\mathrm{max}} - \mathrm{Y}_{\mathrm{min}}}{\mathrm{X}_{\mathrm{max}} - \mathrm{X}_{\mathrm{min}}} \left(\mathrm{x} - \mathrm{x}_{\mathrm{min}} \right) + \mathrm{Y}_{\mathrm{min}}$$

1

To calculate the non-linearity of FD curves, we measured the deviation between the linear line (i.e., ideal curve) and the FD curve (i.e., experimental data);

$$\mathrm{Deviation(D, \backslash\%)} = \frac{\left| \mathrm{y}_{\mathrm{ideal}} - \mathrm{y}_{\mathrm{FD}} \right|}{\mathrm{y}_{\mathrm{ideal}}} \times 100$$

2

Where, y_{ideal} and y_{FD} are y-intercepts of the ideal and experimental data from a FD curve, respectively. We averaged the D in all data points (i.e., sampling number) of the FD curve to calculate the representative non-linearity (*NL*) characteristics for the FD curve.

$$NL = \frac{1}{\mathrm{n}} \sum_{\mathrm{i}=1}^{\mathrm{n}} D_{\mathrm{i}}$$

3

For a certain specimen, hundreds of FD curves are existed, whereby hundreds of *NL* can be calculated. We compared the histograms of *NL* distribution from each specimen as shown in Fig. 5b. Interestingly, we found that the *NL* histograms for normal and benign nevus showed the distribution of less than 40%, whereas the distribution of *NL* histograms for melanoma spreads more than 40%. For more quantitative analysis, we fit the *NL* histograms with the inverse Gaussian distributions given by;

$$\sqrt{\frac{\lambda}{2\pi \mathrm{x}^3}} \exp\left\{ -\frac{\lambda}{2\mu^2 \mathrm{x}} (\mathrm{x} - \mu)^2 \right\}$$

4

Where μ and λ are mean value and the shape parameter of inverse Gaussian distribution. The values of μ were 6.18 ± 1.55, 6.40 ± 1.71, and 8.39 ± 1.38 for normal, nevus, and melanoma, respectively. It shows that the mean value of histograms is increased from normal to benign nevus to melanoma (Fig. 5c), which is attributed to enlarged non-linear characteristics. By contrast, the values of λ were decreased: 5.76 ± 3.06, 5.28 ± 2.15, and 4.80 ± 1.94 for normal, nevus, and melanoma, respectively. Using the value of μ and λ, the standard deviation and the skewness can be calculated through the following two equations:

$$\mathrm{Standard deviation}(\sigma) = \sqrt{\frac{\mu^3}{\lambda}}$$

5

$$\mathrm{Skewness} = 3\sqrt{\frac{\mu}{\lambda}}$$

6

The values of standard deviation (σ) were 61.35 ± 46.03, 54.59 ± 26.47, and 170.04 ± 134.50 for normal, nevus, and melanoma, respectively (Fig. 5d). The standard deviation of *NL* histogram for melanoma was more than twice those of the other two cases (i.e., normal and benign nevus). The values of skewness

also increased from normal to benign to melanoma; 2.90 ± 0.15, 3.46 ± 0.59, and 4.26 ± 1.31, respectively (Fig. 5e). Together, in the melanoma development, all factors for non-linear characteristics (i.e., the values of mean, standard deviation, and skewness of *NL* histograms) were found to be increased compared to the other conditions. It is fair to say that the non-linearity of FD curves can be used as a complementary indicator of discrimination among normal, benign, and melanoma.

Discussion

Using AFM indentation, we characterized the mechanical properties of histological specimens for melanoma detection and discrimination between benign nevus and melanoma. We conclude that the mechanical signatures (the elastic region of E_a and the existence of multiple peaks) for discrimination are universally acceptable regardless of age, sex, or site and that they can specifically demarcate benign nevus versus malignant melanoma samples. In addition, we discover that the non-linearity characteristics of FD curves can be used as a complementary index in collaboration with the elasticity characteristics. From our results, we believe that the AFM indentation of histological specimens provides an excellent complement to histopathological examination for precise diagnosis. Additionally, our method can also be applied as a promising technology not only to determine the safety margin before surgical excision for diagnosis but also to observe the invasiveness during oncological surgery. In the benign nevus, the lesion is relatively easy to be removed without a safety margin but melanoma including both lesion and its borders must be removed for preventing the recurrence or invasiveness of cancer. The accurate diagnosis of the biopsied tissue is expected to reduce the side effects from surgical excisions, such as cancer recurrence, recovery delay, and large surgery scars. Meanwhile, because invasiveness is the important factor for preventing the recurrence, it is determined by using the frozen section method during oncological surgery. Although this method is much easier and faster than with conventional histopathology (around 10 minutes vs. several hours), providing some uncertainty in identifying the invasiveness of cancer. Therefore, our technique can be considered a useful and complementary technique for predicting the invasiveness and ablation margin during oncological surgery.

Declarations

Acknowledgments

This work was supported by the National Research Foundation (NRF) of Korea grant funded by the Korean Government (No. NRF-2018M3C1B7020722, NRF-2019R1A2B5B01070617, NRF-2019R1C1C1005668, and NRF-2020R1A2C2102262). This study was also supported by the BK21 FOUR (Fostering Outstanding Universities for Research) and supported by a grant from Korea University.

Contributions

W.K. and D.L. conceived and designed this manuscript. B.J., J.H.S., M.O.K., B.J.K., S.H.K., and H.L. performed the experiments. H.G.J. and S.W.L wrote the initial manuscript. S.W.L., D.S.Y., S.J.J., and T.H.C

revised and commented on the manuscript. All the authors approved and read the final version of the manuscript.

References

1. Miller , A. J. & Mihm , M. C. J. Melanoma. *N. Engl. J. Med.***355**, 51-65 (2006).
2. Natarajan, V. T., Ganju, P., Ramkumar, A., Grover, R. & Gokhale, R. S. Multifaceted pathways protect human skin from UV radiation. *Nat. Chem. Biol.***10**, 542-551 (2014).
3. Scolyer, R. A., Zhuang, L., Palmer, A. A., Thompson, J. F. & McCarthy, S. W. Combined naevus: a benign lesion frequently misdiagnosed both clinically and pathologically as melanoma. *Pathology***36**, 419-427 (2004).
4. Osborne, J. E., Bourke, J. F., Graham-Brown, R. A. C. & Hutchinson, P. E. False negative clinical diagnoses of malignant melanoma. *Br. J. Dermatol.* **140**, 902-908 (1999).
5. Tannous, Z. S., Mihma, M. C., Flottea, T. J. & Gonzálezb, S. In vivo examination of lentigo maligna and malignant melanoma in situ, lentigo maligna type by near-infrared reflectance confocal microscopy: Comparison of in vivo confocal images with histologic sections. *J. Am. Acad. Dermatol.* **46**, 260-263 (2002).
6. Puig, S. *et al.* Melanomas that failed dermoscopic detection: a combined clinicodermoscopic approach for not missing melanoma. *Dermatol. Surg.* **33**, 1262-1273 (2007).
7. Carli, P. *et al.* The problem of false-positive diagnosis in melanoma screening: the impact of dermoscopy. *Melanoma Res.***13**, 179-182 (2003).
8. Gambichler, T. *et al.* Preoperative Ultrasonic Assessment of Thin Melanocytic Skin Lesions Using a 100-MHz Ultrasound Transducer: A Comparative Study. *Dermatol. Surg.* **33**, 818-824 (2007).
9. Uren, R. F., Sanki, A. & Thompson, J. F. The utility of ultrasound in patients with melanoma. *Expert Rev. Anticancer Ther***7**, 1633-1642 (2007).
10. Celebi, M. E., Iyatomi, H., Schaefer, G. & Stoecker, W. V. Lesion border detection in dermoscopy images. *Comput. Med. Imaging Graph.* **33**, 148-153 (2009).
11. Zhou, H. *et al.* in *Proc. SPIE* 69141B-69141B-69149.
12. Ulrik, B., Erik, B., Peter, Å., Ingrid, N. & Stig, O. Non-invasive bioimpedance of intact skin: mathematical modeling and experiments. *Physiol. Meas.* **32**, 1 (2011).
13. Mohr, P. *et al.* Electrical impedance spectroscopy as a potential adjunct diagnostic tool for cutaneous melanoma. *Skin Res. Technol.* **19**, 75-83 (2013).
14. Glickman, Y. A. *et al.* Electrical impedance scanning: a new approach to skin cancer diagnosis. *Skin Res. Technol.* **9**, 262-268 (2003).
15. Åberg, P., Birgersson, U., Elsner, P., Mohr, P. & Ollmar, S. Electrical impedance spectroscopy and the diagnostic accuracy for malignant melanoma. *Exp. Dermatol.* **20**, 648-652 (2011).
16. Wolf, I. H., Smolle, J., Soyer, H. P. & Kerl, H. Sensitivity in the clinical diagnosis of malignant

17. Simpson, C. L., Patel, D. M. & Green, K. J. Deconstructing the skin: cytoarchitectural determinants of epidermal morphogenesis. *Nat. Rev. Mol. Cell Biol.***12**, 565-580 (2011).
18. Watt, F. M. & Fujiwara, H. Cell-Extracellular Matrix Interactions in Normal and Diseased Skin. *Cold Spring Harbor Perspect. Biol.***3** (2011).
19. Malik, R., Lelkes, P. I. & Cukierman, E. Biomechanical and biochemical remodeling of stromal extracellular matrix in cancer. *Trends Biotechnol.***33**, 230-236 (2015).
20. Gerdes, M. J. *et al.* Emerging Understanding of Multiscale Tumor Heterogeneity. *Front. Oncol.***4** (2014).
21. Provenzano, P. P., Eliceiri, K. W. & Keely, P. J. Shining new light on 3D cell motility and the metastatic process. *Trends Cell Biol.* **19**, 638-648 (2009).
22. Lu, P., Weaver, V. M. & Werb, Z. The extracellular matrix: A dynamic niche in cancer progression. *J. Cell Biol.* **196**, 395-406 (2012).
23. Egeblad, M., Nakasone, E. S. & Werb, Z. Tumors as Organs: Complex Tissues that Interface with the Entire Organism. *Dev. Cell* **18**, 884-901 (2010).
24. Giussani, M., Merlino, G., Cappelletti, V., Tagliabue, E. & Daidone, M. G. Tumor-extracellular matrix interactions: Identification of tools associated with breast cancer progression. *Semin. Cancer Biol.***35**, 3-10 (2015).
25. Raveh Tilleman, T., Tilleman, M. & Neumann, H. The elastic properties of cancerous skin: Poisson's ratio and Young's modulus. *Optimization of Incisions in Cutaneous Surgery including Mohs' Micrographic Surgery.*, 105 (2004).
26. Taloni, A. *et al.* Mechanical Properties of Growing Melanocytic Nevi and the Progression to Melanoma. *PLoS ONE***9**, e94229 (2014).
27. Sarna, M. *et al.* Nanomechanical analysis of pigmented human melanoma cells. *Pigment Cell Melanoma Res.* **26**, 727-730 (2013).
28. Sarna, M. *et al.* Cell elasticity is an important indicator of the metastatic phenotype of melanoma cells. *Exp. Dermatol.***23**, 813-818 (2014).
29. Noonan, F. P. *et al.* Melanoma induction by ultraviolet A but not ultraviolet B radiation requires melanin pigment. *Nat. Commun.* **3**, 884 (2012).
30. Seiberg, M. Keratinocyte–Melanocyte Interactions During Melanosome Transfer. *Pigment Cell Res.***14**, 236-242 (2001).
31. Delevoye, C. Melanin Transfer: The Keratinocytes Are More than Gluttons. *J. Invest. Dermatol.* **134**, 877-879 (2014).
32. He, J. *et al.* Noninvasive, label-free, three-dimensional imaging of melanoma with confocal photothermal microscopy: Differentiate malignant melanoma from benign tumor tissue. *Sci. Rep.***6**, 30209 (2016).
33. Plodinec, M. *et al.* The nanomechanical signature of breast cancer. *Nature Nanotech.***7**, 757-765 (2012).

34. Tian, M. *et al.* The nanomechanical signature of liver cancer tissues and its molecular origin. *Nanoscale***7**, 12998-13010 (2015).
35. Pandya, H. J. *et al.* Accurate characterization of benign and cancerous breast tissues: Aspecific patient studies using piezoresistive microcantilevers. *Biosens. Bioelectron.***63**, 414-424 (2015).
36. Lee, W., Lee, S. W., Lee, G. & Yoon, D. S. Atomic force microscopy analysis of EPPS-Driven degradation and reformation of amyloid-β aggregates. *Journal of Alzheimer's disease reports***2**, 41-49 (2018).
37. Jung, H. G. *et al.* Nanoindentation for Monitoring the Time-Variant Mechanical Strength of Drug-Loaded Collagen Hydrogel Regulated by Hydroxyapatite Nanoparticles. *ACS Omega***6**, 9269-9278, doi:10.1021/acsomega.1c00824 (2021).
38. Lee, D. *et al.* Extremely sensitive and wide-range silver ion detection via assessing the integrated surface potential of a DNA-capped gold nanoparticle. *Nanotechnology***30**, 085501, doi:10.1088/1361-6528/aaf66f (2019).
39. Lee, D. *et al.* Plasmonic nanoparticle amyloid corona for screening Aβ oligomeric aggregate-degrading drugs. *Nature Communications***12**, 639, doi:10.1038/s41467-020-20611-4 (2021).
40. Pogoda, K. *et al.* Depth-sensing analysis of cytoskeleton organization based on AFM data. *Eur. Biophys. J.***41**, 79-87 (2012).
41. Akhtar, R. *et al.* Nanoindentation of histological specimens: Mapping the elastic properties of soft tissues. *J. Mater. Res.***24**, 638-646 (2009).
42. Longo, C., Casari, A., Beretti, F., Cesinaro, A. M. & Pellacani, G. Skin aging: In vivo microscopic assessment of epidermal and dermal changes by means of confocal microscopy. *J. Am. Acad. Dermatol.* **68**, e73-e82 (2013).
43. Cua, A. B., Wilhelm, K.-P. & Maibach, H. I. Elastic properties of human skin: relation to age, sex, and anatomical region. *Arch. Dermatol. Res.* **282**, 283-288 (1990).
44. Chen, K. G. *et al.* Influence of melanosome dynamics on melanoma drug sensitivity. *J. Natl. Cancer Inst.* (2009).

Tables

Table 1. Summary of mechanical analysis and histological examination of biopsied samples with patient information. The corresponding elasticity distributions are shown in Figure S6, S7, and S8).

Case No.	Age/Sex	Biomechanical property			Histopathological diagnosis
		1st peak (0~300 MPa)	2nd peak (300~600 MPa)	3rd peak (600~900 MPa)	
1	4/Male		415±221 MPa		Normal
2	8/Female		401±148 MPa		Normal
3	12/Male		398±252 MPa		Normal
4	32/Male		439±101 MPa		Normal
5	79/Male		521±153 MPa		Normal
6	58/Female		437±261 MPa		Normal
7	3/Male		370±105 MPa		Normal
8	21/Female		485±179 MPa		Intradermal nevus (rt. Thigh)
9	8/Female		450±182 MPa		Congenital melanocytic nevus (lt. Forearm)
10	1/Male		467±178 MPa		Congenital melanocytic nevus (rt. Eyelid)
11	2/Male		441±164 MPa		Congenital melanocytic nevus (rt. Cheek)
12	32/Male		575±107 MPa		Compound nevus (rt. Calf)
13	3/Male		505±162 MPa		Congenital melanocytic nevus (rt. Cheek)
14	13/Female			611±217 MPa	Compound nevus (lt. Cheek)
15	4/Female			848±299 MPa	Congenital melanocytic nevus (rt. Cheek)
16	4/Male			618±187 MPa	Congenital melanocytic nevus (rt. Nasal area)
17	7/Male			636±203 MPa	Congenital melanocytic nevus (rt. Cheek & forearm)
18	8/Male			609±176 MPa	Compound nevus (rt. Cheek)
19	7/Male			650±156 MPa	Congenital melanocytic nevus (rt. Forearm)
20	12/Female			783±177 MPa	Congenital melanocytic nevus (lt. cheek)
21	58/Female	230±49 MPa	483±97 MPa	782±59 MPa	Malignant melanoma, Clark's level I (rt. Cheek)
22	52/Female	158±92 MPa	484±88 MPa	861±58 MPa	Malignant melanoma, Clark's level I (lt. Cheek)
23	81/Female	272±95 MPa	542±80 MPa	893±63 MPa	Malignant melanoma, Clark's level I (lt. Cheek)
24	79/Male	188±79 MPa	497±110 MPa	787±56 MPa	Malignant melanoma, Clark's level IV (lt. Cheek)
25	54/Male			667±221 MPa	Metastatic malignant melanoma, Clark's level IV (lt. Inguinal area)
26	63/Female	211±62 MPa	400±47 MPa	606±19 MPa	Malignant melanoma, Clark's level IV (rt. Thigh)
27	62/Male		373±139 MPa	725±55 MPa	Malignant melanoma, Clark's level IV (lt. Elbow)
28	66/Female	274±93 MPa	475±57 MPa	649±39 MPa	Malignant melanoma, Clark's level IV (rt. Abdomen)
29	55/Female	219±73 MPa	396±43 MPa	610±146 MPa	Malignant melanoma, Clark's level V (lt. Low leg)
30	72/Female	212±40 MPa	486±91 MPa		Malignant melanoma, Clark's level V (lt. Low thigh)
31	56/Female		363±117 MPa	611±39 MPa	Malignant melanoma, Clark's level V (lt. Back)
32	66/Male	227±55 MPa		612±111 MPa	Malignant melanoma, Clark's level V (rt. Flank)
33	79/Male	193±27 MPa	387±49 MPa	767±28 MPa	Malignant melanoma, Clark's level V (rt. Temple)

Figures

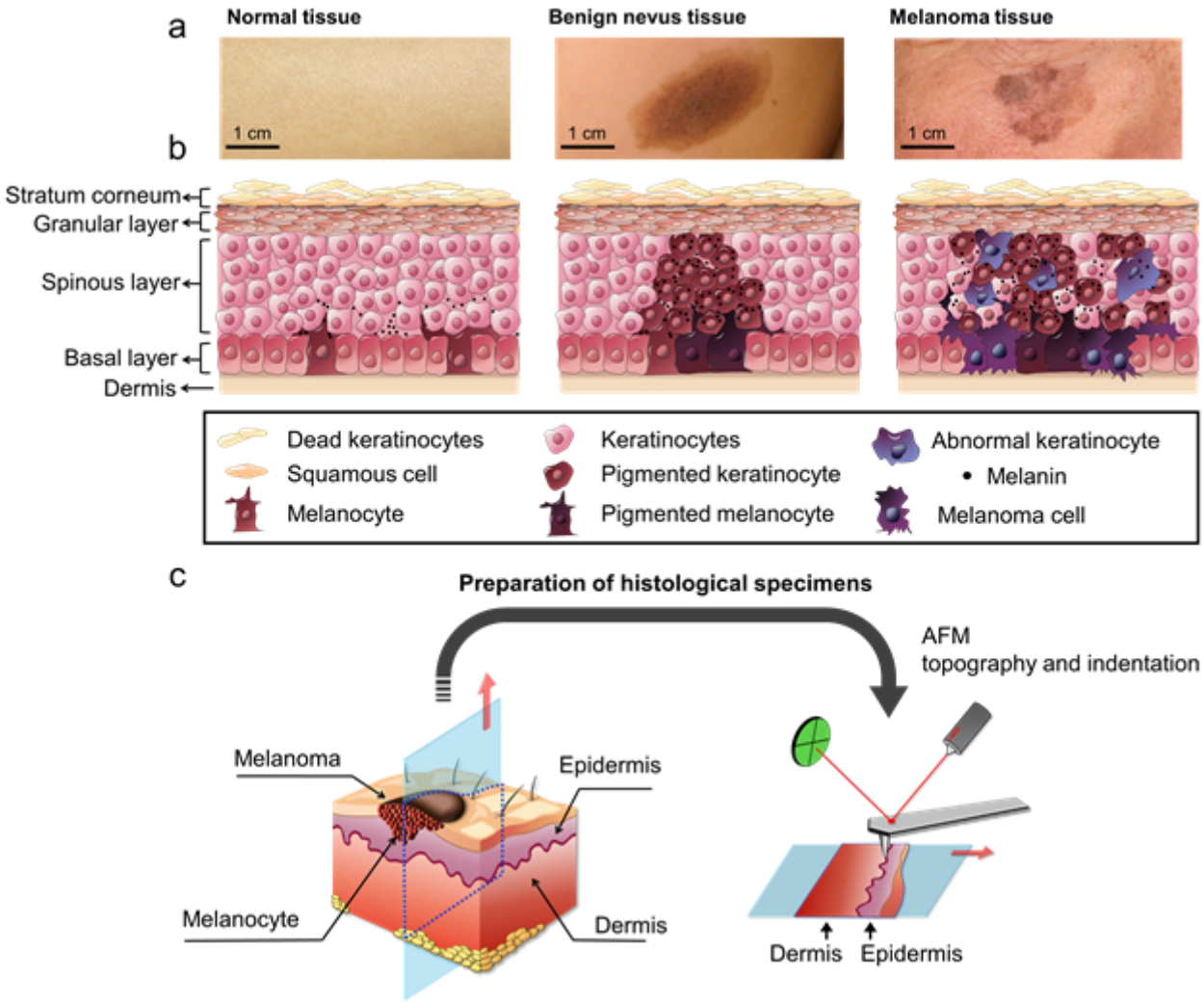

Figure 1

The morphological spectrum and AFM-based analysis of histological specimens. (a) Clinical images of the outermost layer of skin (left to right: normal, benign nevus, melanoma). (b) Schematic illustration of anatomical structures for each type of skin tissue and a rationale of malignant melanoma development with melanin transfer and pigmentation processes in the vicinity of a basal layer. (c) Schematic illustration of tissue biopsy (sampling) and AFM-based analysis.

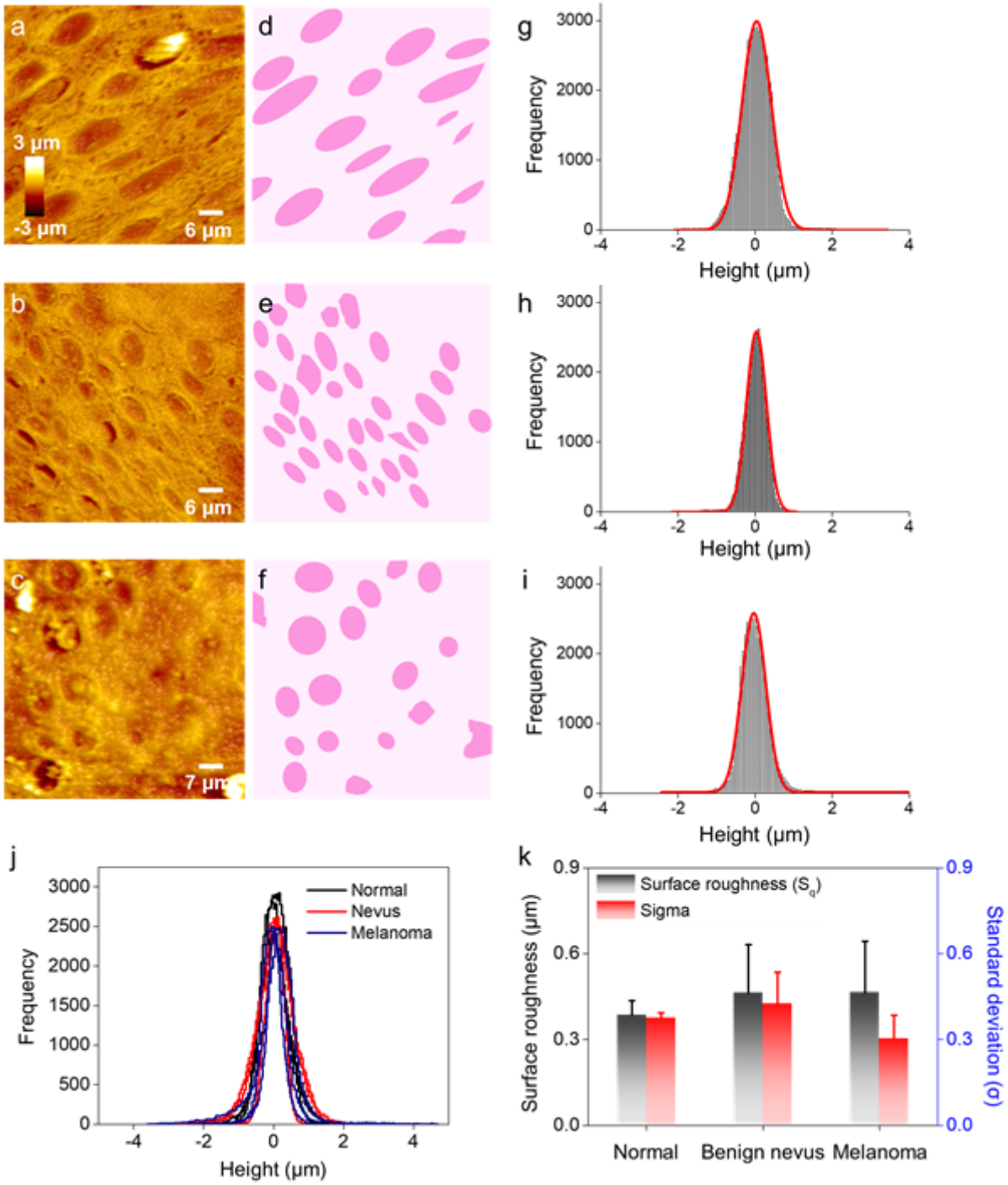

Figure 2

AFM images of (a) normal, (b) benign nevus, and (c) melanoma tissue. (d)-(f) An outlined cell mark obtained from the corresponding AFM images. Statistical height histogram of the AFM images of (g) normal (mean ± standard deviation = 0.03 ± 0.37 μm), (h) benign nevus (0.03 ± 0.25 μm), and (i) melanoma tissue (-0.03 ± 0.31 μm). (j) All height histograms of the normal (solid black line), benign nevus (solid red line), and melanoma (solid blue line) specimens. (k) Mean surface roughness of tissue specimens extracted from AFM image processing program and standard deviation from the Gaussian

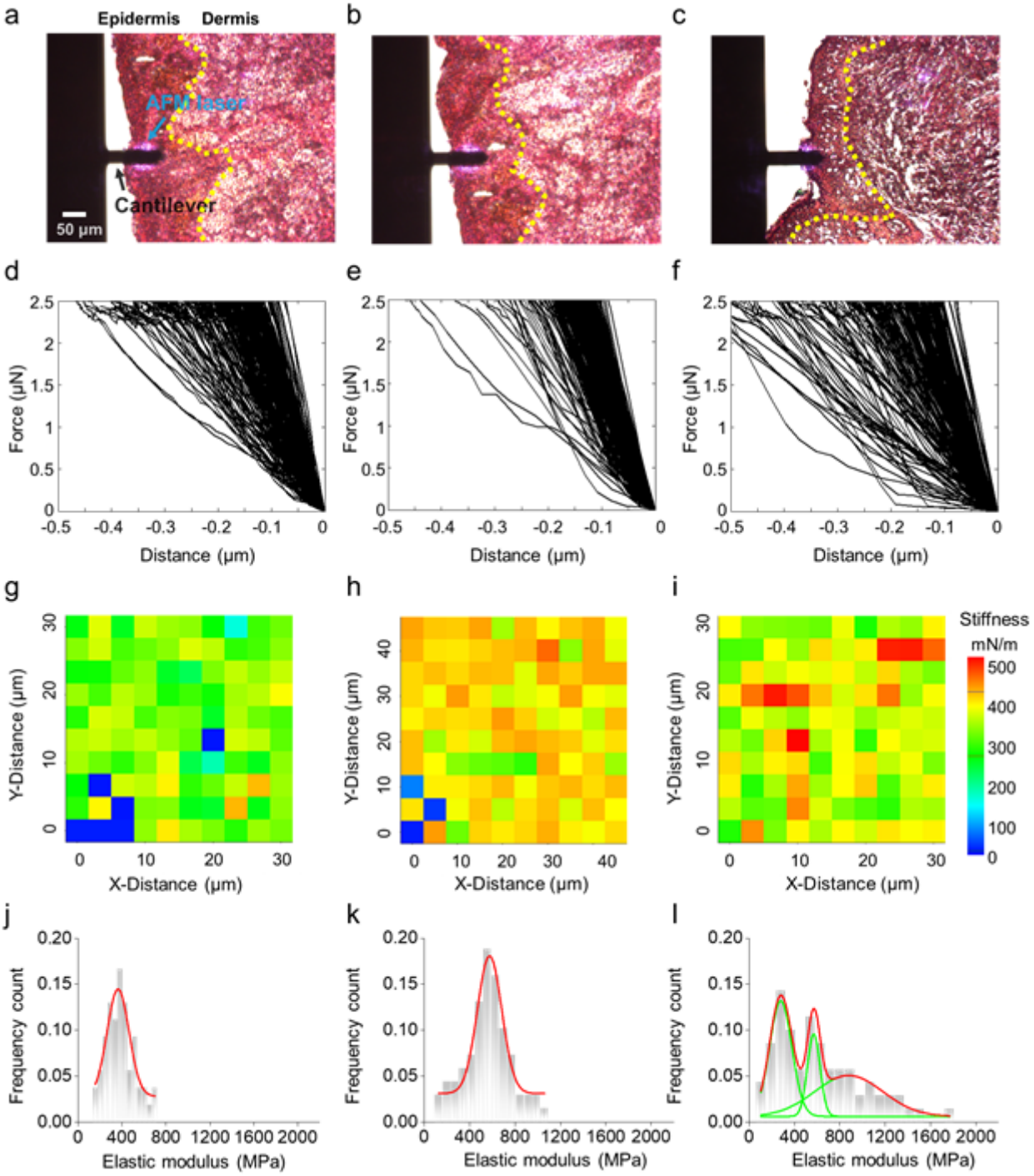

Figure 3

Optical images of the AFM cantilever moved above the tissue on (a) normal, (b) benign nevus, and (c) melanoma specimens. The yellow dotted line indicates a basal layer between the epidermis and dermis. (d)-(f) FD curve and representative stiffness maps (10 × 10 points) across the (g) normal, (h) benign nevus, and (i) melanoma specimens. (j)-(l) Corresponding histogram of elasticity distribution, which was calculated from the FD curve data.

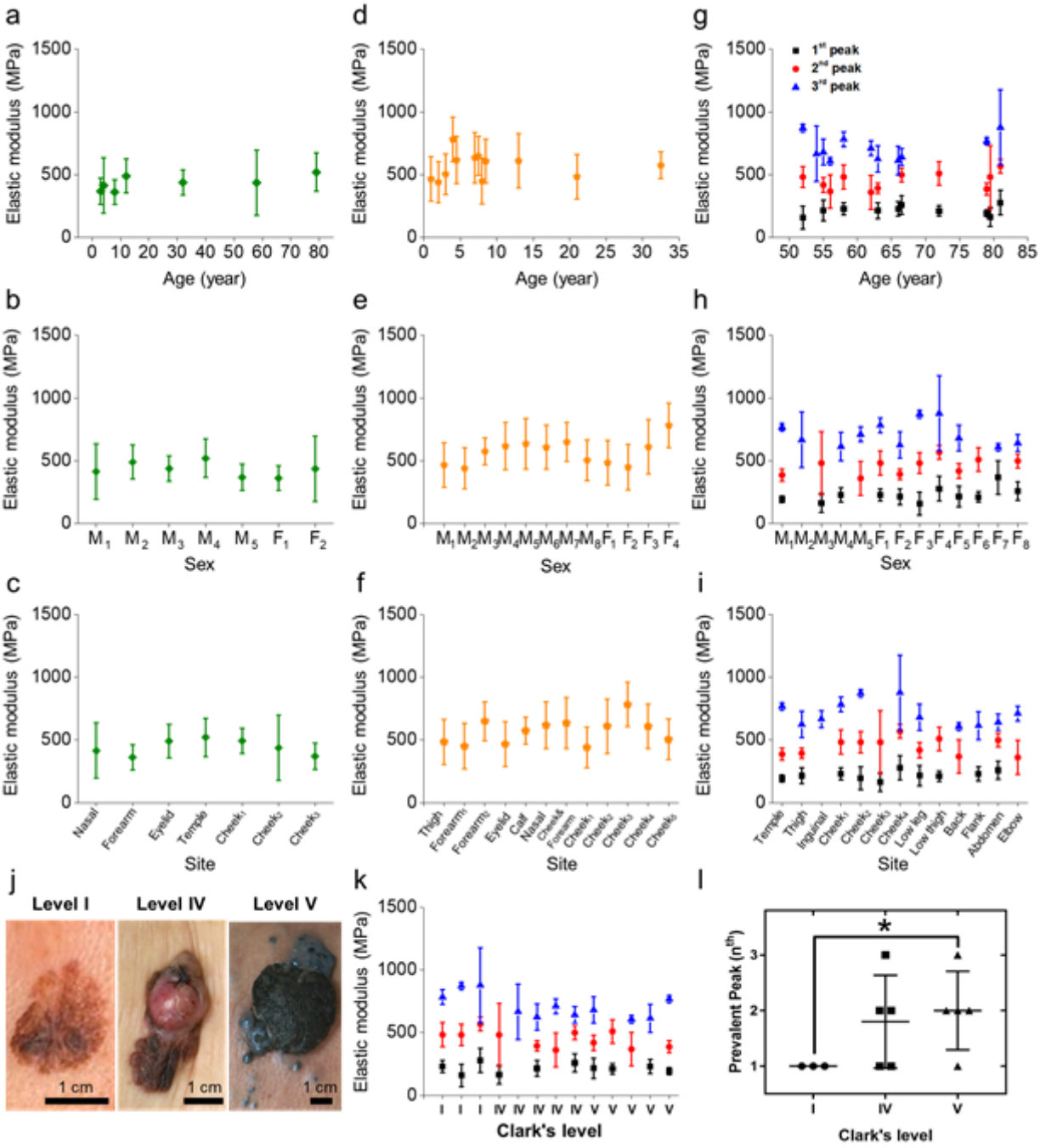

Figure 4

The elasticities of (a)-(c) normal, (d)-(f) benign nevus, and (g)-(i) melanoma specimens are classified by age, sex, and site. (j) Macroscopic images of the different stages of melanoma skin denoted by Clark level. (k) Means and standard deviations for the elasticity of the melanoma tissue specimens by cancer stage. (l) Plot of the prevalent peak range (nth-peak among the first to third peak regions) in elasticity distribution from the histograms (Supplementary Fig. S9), displaying the melanoma development from I to V (*p<0.05).

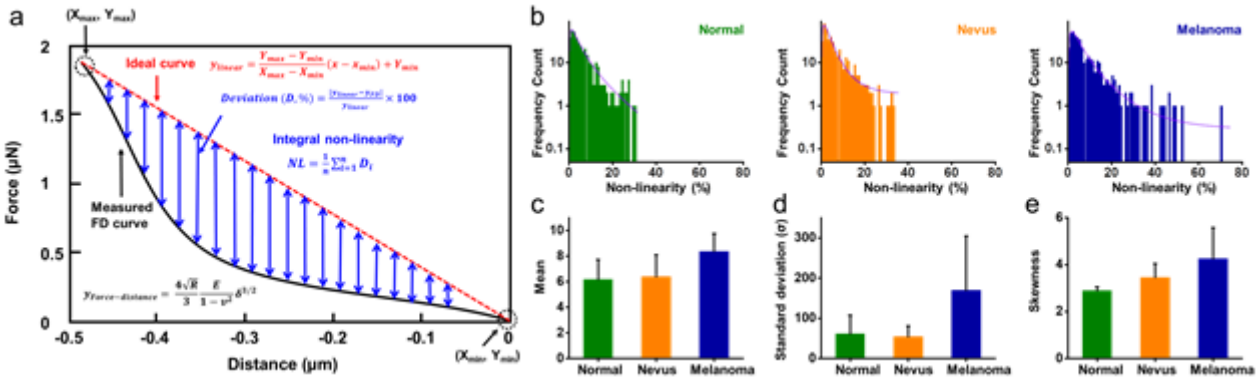

Figure 5

Non-linearity of FD curves of normal, benign nevus, and melanoma specimens. (a) Schematic illustration of calculation of non-linearities. (b) The histograms of non-linearity of normal, benign nevus, and melanoma specimens calculated from individual FD curves. The value of (c) mean, (d) standard deviation, and (e) skewness extracted from a model with the inverse Gaussian distribution of the histograms (b).

Supplementary Files

This is a list of supplementary files associated with this preprint. Click to download.

- SupportingInformation.docx